A sinter resistant Co Fischer-Tropsch catalyst promoted with Ru and supported on titania encapsulated by mesoporous silica

Tumelo N. Phaahlamohlaka[a,c], Mbongiseni W. Dlamini[a,c], Mashikoane W. Mogodi[a], David O. Kumi[a], Linda L. Jewell[b,c], David G. Billing[a], Neil J. Coville[a,c,]

[a] Molecular Sciences Institute, School of Chemistry, University of the Witwatersrand, Johannesburg 2050, South Africa
[b] Department of Chemical Engineering, University of South Africa, Florida, 1710, South Africa
[c] DST-NRF Centre of Excellence in Catalysis South Africa

ARTICLE INFO

Keywords:
Sintering
Cobalt
Reduction
In situ XRD
Fischer-Tropsch synthesis

ABSTRACT

One of the pathways responsible for the deactivation of Fischer-Tropsch catalysts is the loss of active metal surface area due to nanoparticle agglomeration. To combat this effect efforts have been made to increase the interaction between the metal nanoparticles and the support using materials like silica. In this study, the sup-ported metal particles were covered with a highly porous layer of silica to stabilize the Co nanoparticles on a titania support both during reduction and under reaction conditions. Co_3O_4 nanoparticles (size range: 8–12 nm) supported on titania were stabilized by coating them with a thin layer of mesoporous silica (4 nm) to make Fischer-Tropsch catalysts that are less prone to sintering ($Co/TiO_2@mSiO_2$). To mitigate the strong metal sup-port interactions brought about by the titania and silica a Ru promoter was loaded together with the cobalt nanoparticles onto the titania ($CoRu/TiO_2@mSiO_2$). Temperature programmed XRD studies on the evolution of the Co metal nanoparticles showed that there was no significant particle size growth under reduction conditions in the temperature range from 30 to 600 °C. Chemisorption studies following reduction under hydrogen at 350 °C and 450 °C gave results consistent with the in situ XRD data when compared to the Co/TiO_2. Fischer-Tropsch synthesis on the $Co/TiO_2@mSiO_2$ and $CoRu/TiO_2@mSiO_2$ catalysts encapsulated inside the mesoporous silica shell exhibited good catalytic performance without any display of significant mass transport limitations that might arise due to a silica shell coating of the active sites. For these two catalysts the Fischer-Tropsch activity increased with reduction temperature without any significant negative changes in their selectivity due to sin-tering, while the activity on Co/TiO_2 decreased due to Co nanoparticle sintering.

1. Introduction

The Fischer-Tropsch synthesis (FTS) is a key technology in the synthesis of liquid hydrocarbons from gaseous feedstock that can be derived from coal, natural gas and biomass [1,2]. Cobalt metal is the preferred active catalyst in the synthesis of these hydrocarbons by FTS in a hydrogen rich syngas [3–6]. The extended interest in the use of cobalt catalyst for FTS is due to its comparatively higher Fischer-Tropsch activity and lower propensity to catalyze the water gas shift reaction than Fe. It is also highly selective to long chain hydrocarbons that can be easily upgraded to other beneficial products by hydro-cracking [1], and it is economically cheaper in comparison to the other high activity Fischer-Tropsch metals (i.e. Ru).

It is notable that despite more than half a century of research on Co, attempts to control and limit catalyst deactivation during the FT reac-tion and catalyst treatment are still ongoing [6–8]. Amongst the main causes of catalyst deactivation, sintering of cobalt particles under the reaction conditions has been proposed to be one of the major con-tributors in decreasing the Fischer-Tropsch activity of cobalt catalysts [7,9,10]. Catalyst sintering reduces the metal active surface area and can occur by two mechanisms (1) particle coalescence or (2) Ostwald ripening [7]. To combat the deactivation of FTS catalysts by sintering, efforts have been made to increase the interaction between the metal nanoparticles and the support using materials like silica [11,12]. One possibility is to cover the supported metal particles with a highly porous layer that can prevent sintering without inhibiting the catalysis and thus stabilize FTS metal particles during reduction and under reaction conditions.

A number of studies are available in the technical literature that discusses the effects of encapsulation or immobilization of active metal particles using porous oxidic layers to prevent metal nanoparticle sin-tering during catalytic processes [11,13–15]. The positive effect of this

Corresponding author at: Molecular Sciences Institute, School of Chemistry, University of the Witwatersrand, Johannesburg 2050, South Africa E-mail address: neil.coville@wits.ac.za (N.J. Coville).

confinement against metal particle sintering has been validated using several characterization techniques such as XRD, TEM and chemisorp-tion, by comparing the catalysts before and after reaction. Lu et al. [11], observed that a silica layer placed on top of a Pt catalyst supported on TiO_2 greatly enhanced the sinter resistant capabilities of the system. In this case the silica shell was selectively deposited on the TiO_2 supported catalyst to allow sufficient exposure of the metal active sites while serving as a spacer that isolated the individual Pt nanoparticles. The tri-phase (i.e. $Pt/TiO_2@SiO_2$) catalyst displayed good stability up to 800 °C in air for 20 h and showed significant activity in the p-nitrophenol re-duction reaction using sodium borohydride. A TEM analysis study performed by Chen and co-workers for example, [14], showed that the oxide shell coating methodology could also be extended to non-noble metal catalysts. CuO nanoclusters with an approximate size of 60 nm synthesized by a solvothermal method and then coated with a meso-porous silica shell were compared with non-coated nanoclusters. The two nanoclusters were tested for olefin (norbornene) epoxidation over a period of time and a number of cycles. The $CuO@meso\text{-}SiO_2$ remained unchanged after an 8 h epoxidation reaction, whereas the CuO na-noclusters underwent severe sintering only after 4 h of reaction. Fur-thermore, an epoxidation reaction on $CuO@mSiO_2$ for 720 h did not show any significant catalyst particle aggregation. Similar procedures for preventing nanoparticle sintering have also been applied to bime-tallic catalysts, such as Pt-Co nanoparticles for the oxygen reduction reaction (ORR) [16]. Pt_3Co nanoparticles were coated by a silica shell and they were supported on carbon materials. High temperature an-nealing at 800 °C under 10% H_2/Ar to allow sufficient alloying did not show any metal particle agglomeration. The $Pt_3Co@SiO_2/C$ was com-pared using PXRD with an uncoated Pt_3Co/C catalyst after annealing at 800 °C and showed crystallite sizes of 3.1 nm and 24.6 nm, respectively, while the original Pt_3Co crystallite sizes were in the range of 2–4 nm. This showed that the silica shell served as a structural stabilizer for preserving the original nanoparticle size and that alloy formation was not hampered. A number of other oxides such as, ceria and titania have also been used to similar effect as structural promoters and stabilizers to reduce metal nanoparticle sintering [13,17,18]. Reddy et al. [17], used a thin layer of TiO_2 to stabilize Pt nanoparticles supported on silica spheres. The $Pt/SiO_2@TiO_2$ composite retained its morphology and shape even after calcination at 600 °C in air with no apparent increase in Pt particle size. A high metallic dispersion of 53% was retained during a CO oxidation reaction demonstrating that the titania shell still allowed diffusion of reactants. These studies therefore demonstrate that coating active metal particles with a protective layer can limit the sintering of nanoparticles during catalyst pre-treatment and testing.

In this study we extend this protocol by preparing Co catalysts for FTS to study the effect of coating the supported cobalt nanoparticles with a mesoporous silica shell to limit the metal nanoparticle growth during reduction and under FT conditions. The activity of uncoated cobalt catalysts was compared with that of cobalt catalysts en-capsulated with a silica shell to determine whether the increased metal interactions would (1) reduce sintering (2) lower the catalyst catalytic activity.

2. Experimental

2.1. Chemicals

Titania (TiO_2; Degusa), tetraethylorthosilicate (TEOS 98%; Aldrich), ammonia solution (25%; Fluka), hexadecyltrimethylammonium bro-mide (CTAB; Aldrich), ruthenium chloride (Aldrich), urea (Promark chemicals), ethanol (98%; Merck) and cobalt (II) acetylacetonate (Aldrich) were used as received. Deionized water was used in the ex-periments.

2.2. Preparation of the cobalt supported on titania

Co/TiO_2: Cobalt particles (10% wt) were loaded on the titania support using homogeneous deposition precipitation. Titania (10 g) was dispersed in 450 mL of water, and cobalt (II) acetylacetonate (4.363 g) and urea (0.4 g) were added and then dispersed by sonication for 20 min. Deposition of the Co particles was performed for 18 h at 95 °C using the slow decomposition of the urea, which served as the pre-cipitating agent. After precipitation the slurry solution was then dried at 65 °C using a rotary evaporator. The sample was then dried at 100 °C

$CoRu/TiO_2$: Preparation of the Ru promoted catalyst was prepared using the same method, but in this case the concentrations of the so-lution were calculated to give a loading of 9.5% and 0.5% cobalt and ruthenium using cobalt (II) acetylacetonate (4.145 g) and ruthenium chloride solution (0.1 M, 4.95 mL).

Calcination of the prepared samples was performed at 250 °C under static air for 2 h.

2.3. Coating of the Co/TiO_2 and $CoRu/TiO_2$ with a mesoporous silica shell

Coating of the Co/TiO_2 or $CoRu/TiO_2$ catalyst precursors was done using TEOS as the silica source and CTAB as the surfactant. Co/TiO_2 (4 g) was dispersed in 150 mL of ethanol by sonication for 30 min. To this solution was added ammonia solution (1 mL). TEOS (2 mL) and CTAB (3g) in ethanol (50 mL) was then slowly added into the mixture while stirring to generate the silica shell. The resulting solution was aged while stirring at room temperature for 12 h to allow complete precipitation of the TEOS. The product was then filtered by vacuum filtration and then washed with acetone followed by drying of the solid product at 100 °C overnight.

The samples were calcined at 500 °C for 4 h under static air.

The materials obtained were called $CoRu/TiO_2@mSiO_2$ and $Co/TiO_2@mSiO_2$ (i.e mesoporous silica encapsulated Co or CoRu sup-ported on titania, see Fig. 1).

2.4. Material characterization

TEM analysis was performed on a Tecnai spirit (T12) transmission electron microscope operating at 120 kV. The samples were dispersed in methanol by ultrasonication and loaded onto a copper grid. The bulk composition of the catalysts was analyzed using a Bruker D2 phaser equipped with a Lynxeye detector. Co-Kα radiation was used at 30 kV. The scan ranged from 10 to 90° 2θ in 0.0260 steps. Data obtained from in situ PXRD studies are given in the Supplementary section. N_2 ad-sorption–desorption experiments were conducted at 195 °C using a Micromeritics Tristar 3000 surface area and porosity analyzer. Prior to

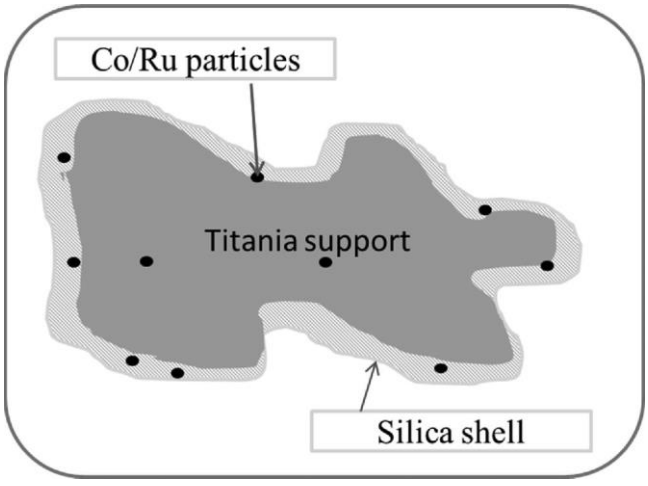

Fig. 1. Cartoon showing the $CoRu/TiO_2@mSiO_2$ three-phase material architecture

an experiment, the sample was outgassed at 150 °C for 4 h under ni-trogen gas. The BET surface areas were obtained from the adsorption data in a relative pressure range from 0.05 to 0.30. The total pore vo-lumes were calculated from the amount of N_2 vapor adsorbed at a re-lative pressure of 0.99. The pore size distributions were evaluated from the desorption branches of the isotherms using the Barrett–Joyner–Halenda (BJH) method. The micropore area and vo-lume were calculated using the t-plot data. The TPR experiments were carried out with a Micromeritics Auto Chem II unit. The catalyst (ap-proximately 0.1 g) was placed in a quartz tubular reactor which was fitted with a thermocouple for continuous temperature measurement. The reactor was heated in a furnace. Prior to the temperature-pro-grammed reduction measurement, the calcined catalysts were flushed with high-purity argon at 150 °C for 1 h, to remove water or impurities followed by cooling to ambient temperature. Then, 5% H_2/Ar was switched on, and the temperature was raised at a rate of 10 °C min^{-1} from 50 to 900 °C. The gas flow rate through the reactor was controlled by three Brooks mass flow controllers and was always 50 mL min^{-1}. The H_2 consumption (TCD signal) was recorded automatically by a computer. Pulse chemisorption was performed using the Micromeritics Auto Chem II instrument to give the number of active metal atoms. The catalyst (ca. 0.2 g) was placed in a quartz tubular reactor. The sample was reduced at 350 or 450 °C for 2 h under a hydrogen flow of 50 mL min^{-1}. Before injecting the adsorbent gas, the sample was purged using helium gas at 350 °C for 1 h, followed by cooling to am-bient conditions. Hydrogen chemisorption (assuming a H/Co ratio of 1) was then performed at 150 °C using ultra-pure hydrogen as the active gas and argon as the carrier gas.

2.5. Evaluation of Fischer-Tropsch synthesis reaction

The Fischer–Tropsch synthesis was performed in a fixed-bed micro-reactor (internal diameter = 1.6 cm and length = 25 cm). A gas cy-linder containing H_2/CO/N_2 mixtures (60/30/10 vol.% purity: 99.99) was used to supply the reactant gas stream to the catalyst at a flow rate of 20 mL/min. N_2 was used as an internal standard in order to ensure accurate mass balances. Catalyst (1.5 g) was added to the reactor and reduced in situ at 350 °C or 450 °C for 2 h under a stream of H_2 (1.5 bar at 50 mL min^{-1}). After reduction, the reactor temperature was de-creased to ambient temperature under a hydrogen flow, then heated up to 220 or 250 °C under synthesis gas at a pressure of 10 bar. All gas lines after the reactor were kept at 100 °C, and a hot trap placed immediately after the reactor was held at 150 °C in order to collect wax. A second trap kept at ambient temperature was used to collect the oil and water mixture. The flow was controlled using a metering valve and measured by a bubble meter. The product stream was analyzed online using two gas chromatographs. A thermal conductivity detector (TCD), equipped with a Porapak Q (1.50 m × 3 mm) packed column, was used to analyze H_2, N_2, CO and a flame ionization detector (FID), equipped with a Porapak Q packed column was used for the online analysis of hydro-carbons. Hydrocarbons collected in the knockout pots were analyzed using an offline GC, equipped with a ZB-1 packed column.

3. Results and discussion

3.1. Catalyst structure characterization

The Co particle loading was performed using the homogenous de-position precipitation (HDP) method, a common method employed for catalyst preparation to give uniform particle sizes [19]. TEM analysis of the catalyst particles on titania displayed a uniform size with an average of about 10.1 nm after calcination at 250 °C (Fig. 2). The target Co loading was 10%.

Fig. 3, shows TEM images of the catalysts that were made by adding TEOS/CTAB onto the Co/TiO_2 and CoRu/TiO_2. It is clear that a suc-cessful coverage of the Co/TiO_2 composite with a mesoporous silic shell was obtained (Fig. 3c) and the silica shell thickness was found to be 4 nm. The coverage of titania with a silica shell is well documented in the literature as the oxidic interaction of the silica and titania to form this type of composite is thermodynamically favored making the pro-cess of coating the Co catalysts a facile one [20]. The porogen CTAB was removed from the silica shell by calcination at 500 °C for four hours. Little sintering of the Co_3O_4 occurred on calcination at 500 °Cas shown by the XRD line broadening analysis of crystallite sizes (see Fig. S.1 and the accompanying Table to Fig. S.2). A slight growth of Co_3O_4 catalysts (from 10.3 nm to 11.8 nm) on the silica coated catalysts during calcination at 500 °C occurred during the CTAB removal process. The growth was more significant (from 10.3 nm to 12.9 nm) when the un-coated catalyst (Co/TiO_2) was calcined at 500 °C. The difference is not large showing that sintering of Co_3O_4 is not substantially affected by the silica overlayer.

Porosity analysis of the catalyst precursors was performed by using the nitrogen adsorption-desorption method (Table 1 and Fig. S.3). It was observed that the silica coating was mesoporous as confirmed by the increased BET surface area of the silica coated catalysts to 103 m^2 g^{-1} and 113 m^2 g^{-1} for Co/TiO_2@mSiO_2 and CoRu/TiO_2@ mSiO_2 respectively when compared to the BET surface area of the un-coated Co/TiO_2 of 56 m^2 g^{-1}. It can therefore be inferred that the mesoporous silica shell with a thickness of approximately 4 nm and a percentage loading of 11.7% contributed to more than 40% of the coated catalyst's BET surface area. The mesoporous silica shell's surface area was estimated to be > 450 m^2 g^{-1} as determined from this equa-tion:

$$T_{SSA}\ (m^2/g) = SSA\ (Co/TiO_2) \times \chi_{Co/TiO2} + SSA\ (mSiO_2) \times \chi_{mSiO2}$$

where T_{SSA} is the total BET surface area, SSA (Co/TiO_2) and SSA (mSiO_2) are the specific surface areas of the Co/TiO_2 and the mesoporous silica shell respectively, and χ (x) refer to weight fractions The increased surface area after coating with the silica suggests that the catalysts are effect of the silica shell The porous silica shell was formed by removal of the porogen sufficiently porous to allow the encapsulated Co nano-particles to interact with the synthesis gas during the Fischer-Tropsch synthesis. Further, the nanoparticle surface mobility would be expected to be hindered by the encapsulating (CTAB) during the calcination process [21].

3.2. Catalyst dispersion

Pulse chemisorption studies were performed to determine the dis-persion of the Co nanoparticles on the support at two reduction tem-peratures (350 and 450 °C; Table 2 and Fig. S.4). The estimated dis-persions were in the range of 1–7%. Fischer-Tropsch catalysts supported on oxidic supports are generally observed to have low dis-persions [22]. It should however be noted that the low dispersions observed can be due to two effects; large particle sizes or strong metal support interactions (SMSI) [22]. Promotion of Co by a Ru promoter can facilitate the reduction of cobalt oxide e.g. in CoRu/TiO_2@mSiO_2 relative to the cobalt oxide in Co/TiO_2@mSiO_2.

The degree of reduction (DOR) for the catalysts was estimated by pulse chemisorption using oxygen at 400 °C after reduction at 350 and 450 °C (Fig. S.5) [23]. The data at 350 °C for Co/TiO_2 and Co/TiO_2@ mSiO_2 showed that the silica only had a small effect (decrease) on the reducibility of Co (49% vs 44%). This would suggest that the Co-titania interaction is (as expected) more dominant in terms of affecting the reduction behavior of Co than the interaction between Co and the meso porous silica layer. The DOR of the CoRu/TiO_2@mSiO_2 relative to that of Co/TiO_2@mSiO_2 (350 °C) only showed a small increase (44%–48%) again suggesting a dominance of the Co-TiO_2 interaction at this low reduction temperature.

At a higher reduction temperature (450 °C) similar results were obtained but at a higher DOR. Given the hydrogen chemisorption

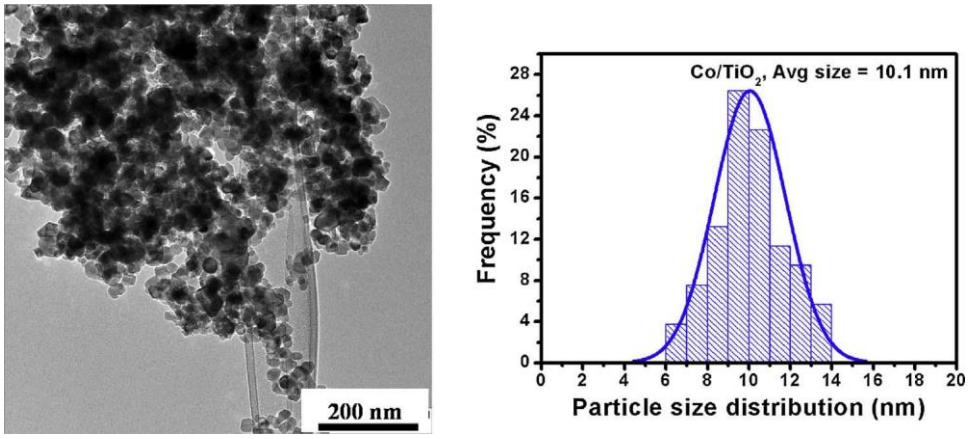

Fig. 2. TEM image and Co_3O_4 particle size distribu-tion of Co/TiO_2.

experiement was performed at 150 °C, at this temperature the different metal support interaction (i.e. TiO_x and SiO_x species) also attenuate the Co surface atom interactions with hydrogen [5,22,24].

The dispersion data for the three catalysts (both uncorrected and corrected for degree of reduction) are shown in Table 2. The dispersion data (Table 2) show the contrasting effects associated with particle sintering and metal-support interactions. Firstly, as expected, for Co/TiO_2 the dispersion decreased as the reduction temperature increased from 350 °C to 450 °C. This can be attributed to particle sintering of the uncoated Co nanoparticles at 450 °C leading to a lower metallic surface area. In contrast, the dispersion of $Co/TiO_2@mSiO_2$ remained almost the same (3.6% vs. 3.7%) with an increase in temperature suggesting little or no sintering of the Co. Finally, the $CoRu/TiO_2@mSiO_2$ showed an increase in dispersion with temperature. Here the ability of the Ru to enhance the reducibility of the Co has increased with temperature and sintering also appears to have been limited. The corrected values for the dispersion (6.7% vs. 3.7%) are also consistent with this suggestion.

3.3. Catalyst reduction

3.3.1. Temperature programmed reduction (TPR)

TPR studies were used to provide information about the reducibility of the supported cobalt oxide nanoparticles. Displayed in Fig. 4(a) are the reduction profiles of the three catalyst precursors under a flow of

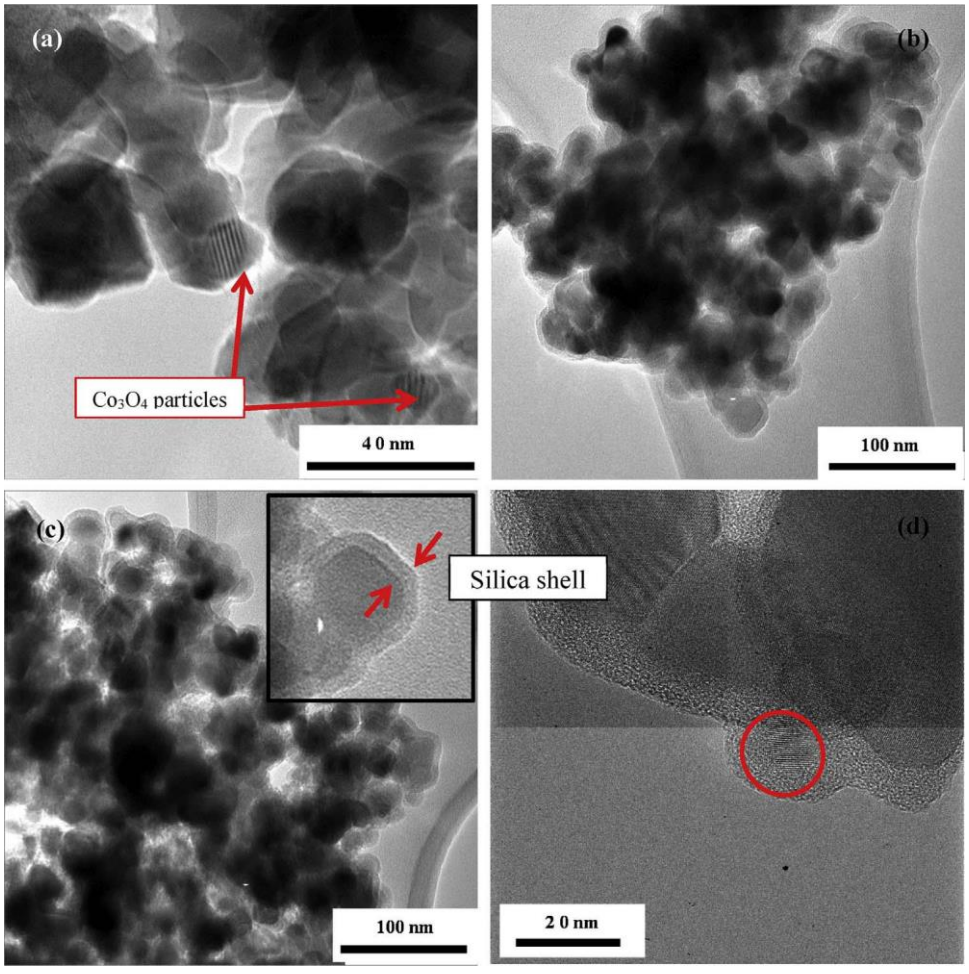

Fig. 3. TEM images of the catalysts. (a) Co/TiO_2, (b) $Co/TiO_2@mSiO_2$, (c) $CoRu/TiO_2@mSiO_2$, inset: magnified image showing the silica shell on the ti-tania, (d) micrograph showing an encapsulated Co_3O_4 nanoparticle.

Table 1
Physical properties of the catalysts.

Sample name	BET surface area (m^2/g)	Pore volume (cm^3/g)	Silica loading (%)[a]	Cobalt loading (%)[a]	Ruthenium loading(%)[a]
Co/TiO_2	56	0.289	0	10	0
Co/TiO_2@ $mSiO_2$	103	0.398	11.65	8.83	0
CoRu/ TiO_2@ $mSiO_2$	113	0.348	11.65	8.39	0.44

[a] Estimated based on the amount of material precursor used.

Table 2
Pulse Chemisorption data recorded at 150 °C.

	CoRu/TiO_2@ $mSiO_2$		Co/TiO_2@$mSiO_2$		Co/TiO_2	
Reduction temperature (°C)	450	350	450	350	450	350
Corrected active site (nm)	14.9	19.8	28.0	25.8	52.4	22.2
DOR (%)	59	48	57	44	60	49
Dispersion (%)	3.9	2.4	2.1	1.6	1.1	2.2
Corrected dispersion (%)	6.7	5.0	3.7	3.6	1.9	4.5

5% H_2/Ar. The TPR profile of Co/TiO_2 showed the two distinct re-duction peaks characteristic of the Co oxide spinel phase. These re-duction peaks correspond to the following phase transitions (i) $Co_3O_4 \rightarrow CoO$ and (ii) $CoO \rightarrow Co$ at 320 °C and 490 °C respectively. In compar-ison, the interaction of a silica shell on the Co/TiO_2 catalyst increased the reduction temperatures for these transitions (350 and 540 °C) due to the increased metal support interactions induced by the oxidic silica shell [5,22,25,26]. A peak between 550 and 700 °C is also observed, presumably due to spinel formation of cobalt silicates and titanates mixed metal oxides. To mitigate this problem reduction promoters using noble metals can be used to lower the reduction temperatures of the catalysts [5,27]. The reduction of the catalyst $CoRu/TiO_2$@$mSiO_2$ was achieved at lower temperatures (< 400 °C). This reduction did not occur by formation of a stable CoO intermediate since the two reduction peaks overlap. This may be due to the increased kinetics of the reduc-tion of the Co oxides that is promoted by the Ru promoter via a hy-drogen spillover process or even direct Co-Ru interactions [28–30]. The reduction of the catalyst precursors is summarized in the scheme in Fig. 4(b) showing the dependency of the Co oxide reduction on silica shell and the Ru promoter.

3.3.2. In situ PXRD analysis

3.3.2.1. Phase transformation. The catalysts were studied in situ using variable temperature PXRD to determine the evolution of the Co particles during the reduction process. This method was also used to ascertain that the silica shell off ered some stability to the supported Co

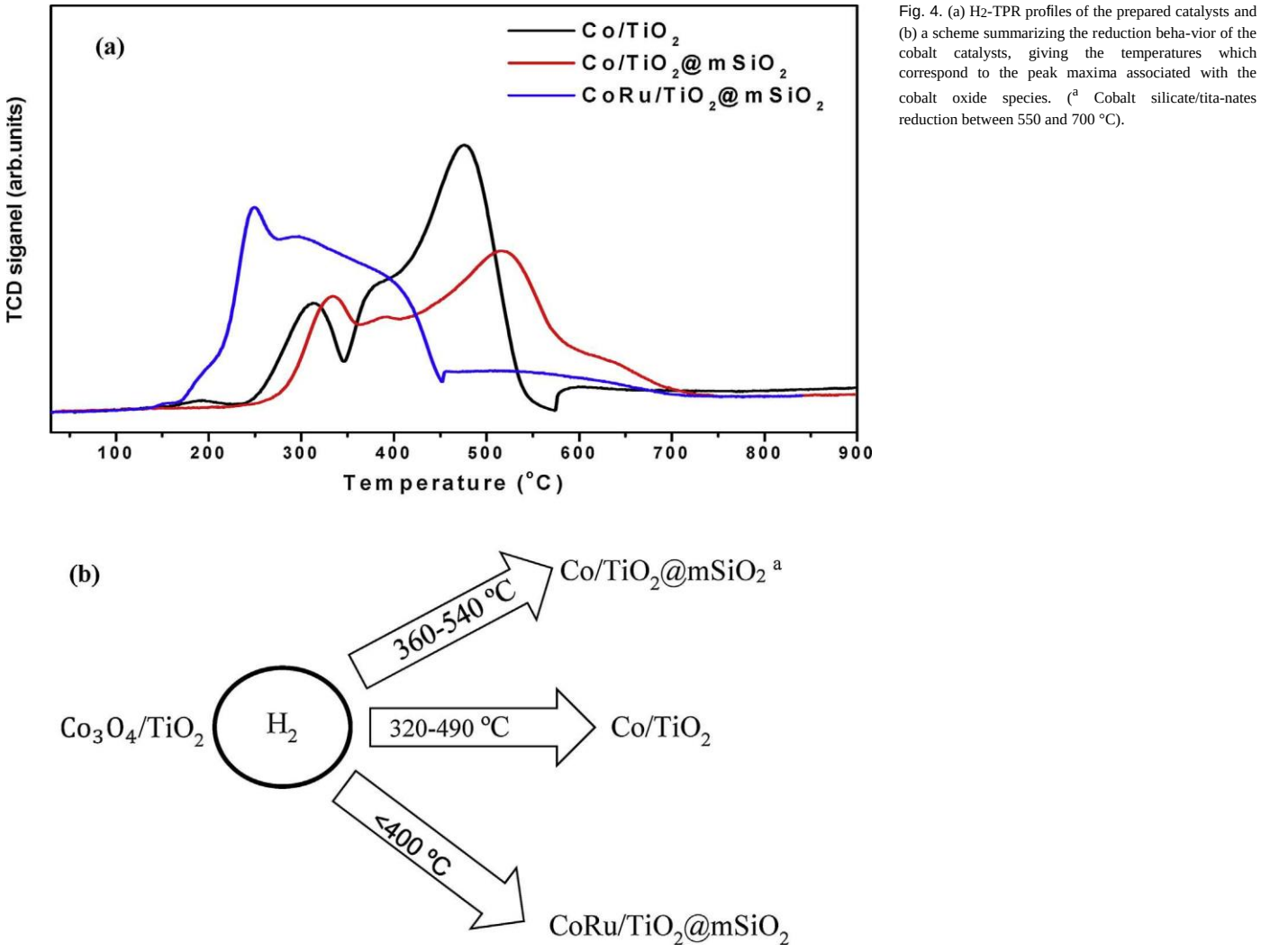

Fig. 4. (a) H_2-TPR profiles of the prepared catalysts and (b) a scheme summarizing the reduction beha-vior of the cobalt catalysts, giving the temperatures which correspond to the peak maxima associated with the cobalt oxide species. ([a] Cobalt silicate/tita-nates reduction between 550 and 700 °C).

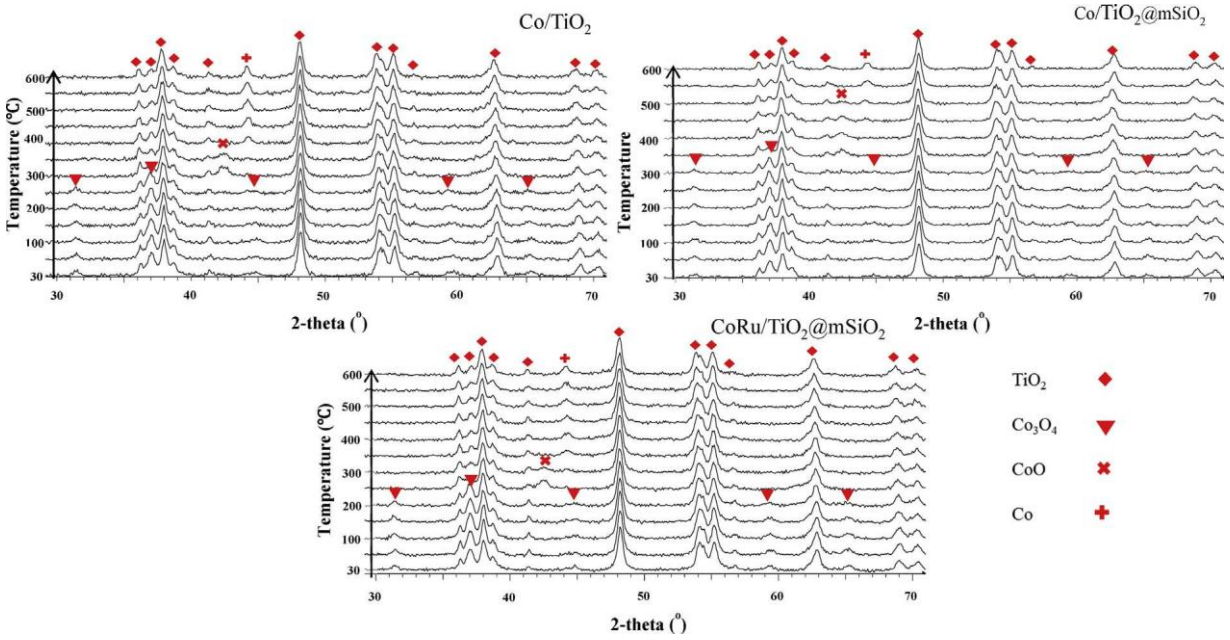

Fig. 5. In situ PXRD patterns for the catalysts recorded under reduction conditions at ambient pressure.

nanoparticles against sintering at high reduction temperatures.

The step-wise reduction of the catalysts was monitored under PXRD from 50 to 600 °C in 50 °C intervals in a 5% H_2/N_2 gas mixture (Figs. 5 and S.6, and Table S.1). The reduction behavior of the catalysts vali-dated the data observed in the temperature programmed reduction study.

The PXRD patterns confirmed the two stage Co oxide phase trans-formation and showed that almost complete reduction of the catalysts occurred below 600 °C. The anatase phase of the support did not un-dergo any phase transformation to rutile under these non-ambient conditions.

The Co/TiO_2 catalysts displayed complete transformation of Co_3O_4 to CoO at 300 °C while the same transformation for the silica en-capsulated Co/TiO_2 commenced at 350 °C. This transformation was also observed at lower temperatures (250 °C) for the Ru promoted silica encapsulated Co/TiO_2 (i.e. $CoRu/TiO_2$) possibly due to the effect of a hydrogen spillover process. The reduction of the CoO intermediate was also accelerated as seen by the subsequent conversion to Co at 300 °C. The total reduction of CoO to Co for Co/TiO_2 and $Co/TiO_2@mSiO_2$ were observed at 450 and 500 °C respectively.

The Ru promoter reduced the reduction temperature by ±100 °C while the use of the $mSiO_2$ as the structural promoter (without a re-duction promoter) raised the reduction temperature of the catalyst by ± 50 °C. Fig. 6 also displays the relative abundance of the Co phases as calculated by Reitveld refinement using the fundamental parameter approach [31]. The degree of reduction (DOR) of these catalysts based on the relative percentage of the Co phase, was indeed hampered by the silica shell. This was confirmed from the XRD patterns collected at 450 °C for both Co/TiO_2 and $Co/TiO_2@mSiO_2$. At this temperature the catalysts have a DOR of 100% and 13% respectively (Fig. 6a and b), hence attesting to the increased metal support interactions on the structurally promoted catalyst. However, these effects were offset by the Ru promoter as the $CoRu/TiO_2@mSiO_2$ was observed to give 100% reduction at a lower temperature of 350 °C (Fig. 6(c)) [22,26,32].

3.3.2.2. Particle size evolution upon reduction. In situ XRD data were collected using an XRK cell and quantitative phase analysis was done by Rietveld refinement (Fig. S.7) to study the cobalt particle size variation on the three catalysts during reduction (using 5% H_2 nitrogen) from 50 °C to 600 °C [33–35]. Silica coated catalysts (i.e. $CoRu/TiO_2@mSiO_2$ and $Co/TiO_2@mSiO_2$) did not show significant particle growth during the process (Fig. 6 and Table S.1). The estimated Co_3O_4 crystallite sizes (calculated using the Rietveld refinement method from the XRD patterns) were in the range of 10–12 nm for both $CoRu/TiO_2@mSiO_2$ and $Co/TiO_2@mSiO_2$. After phase transformation to CoO at elevated temperatures the sizes were observed to be ca. 9.4 nm and between 8.5 and 9.3 nm respectively. Further reduction of these samples to form the Co cubic phase resulted in a further decrease of the estimated sizes to approximately 7.5 to 8 nm and 9–10 nm for $CoRu/TiO_2@mSiO_2$ and $Co/TiO_2@mSiO_2$ respectively. At temperatures above 550 °C a slight increase in the Co crystallite sizes was observed indicating modest sintering at elevated temperatures. For the uncoated Co/TiO_2 catalyst the Co particles sizes were found to vary: for Co_3O_4 the crystallite size was between 10 and 11 nm and ca. 8 to 9 nm for the CoO phase. However, the Co phase crystallite sizes were observed to range from 8.9 to 16.2 nm at temperatures between 400 and 600 °C.

The in situ PXRD studies and refinement analysis of the diffraction patterns showed that due to the increasing SMSI and possible formation of amorphous Co with increasing temperature the Co peak intensity decreased with increasing reduction temperature [34].

The slight growth of the Co crystallites on the silica coated catalysts may also be related to the SiO_2 layer thickness, as was observed by Lu et al. [11]. Here it was shown that a thicker silica shell offered more nanoparticle stabilization than a thin silica shell when the temperature was ramped up to elevated temperatures (i.e. 800 °C). In our study the silica shell was approximately 4 nm in thickness. It is possible that a thicker silica layer will further stabilize the Co nanoparticles. However, this could lead to a less active Co catalyst, if it covers the particles completely or results in SMSI leading to the formation of cobalt sili-cates.

3.4. Fischer Tropsch synthesis study

3.4.1. Activity

Evaluation of the FTS activity to decipher the effect of the promoters on the catalysts was performed at 220 and 250 °C for 50 h at each re-action temperature. Pre-treatment of the three catalysts was done by reduction at different temperatures (350 and 450 °C) to observe the effect of the different reduction temperatures on the catalyst activity. Increased FT activity (see Table 3, Fig. S.8) in terms of CO conversion

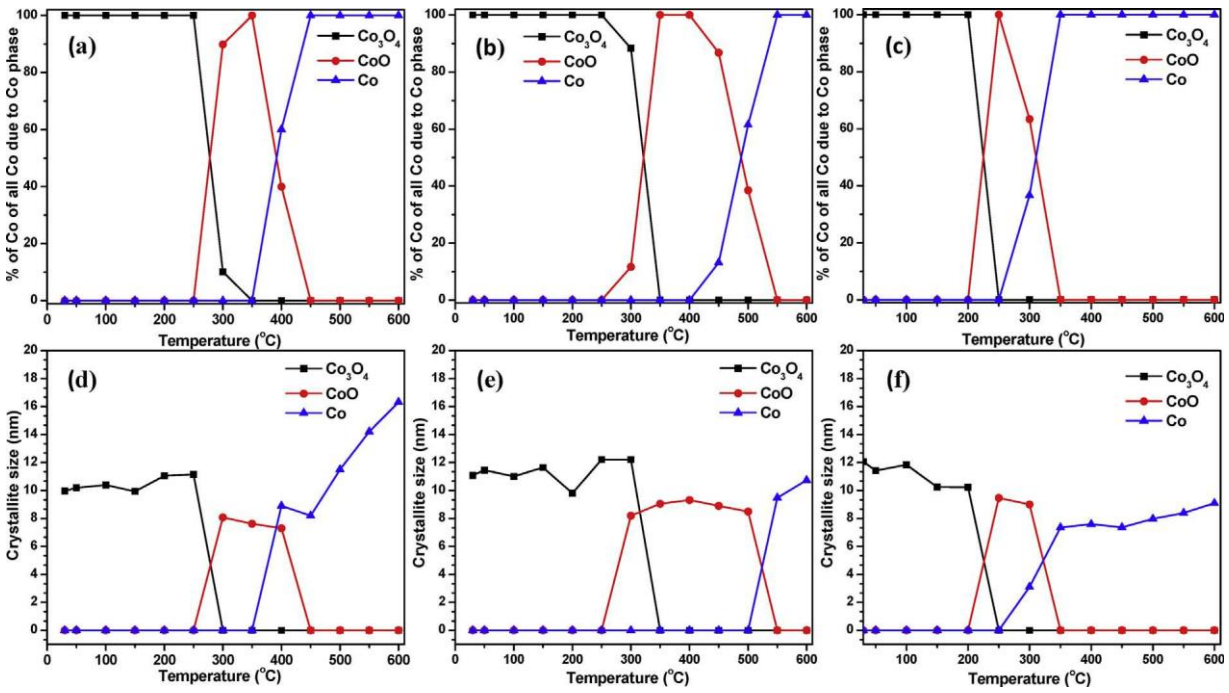

Fig. 6. Abundance and crystallite size changes of Co_3O_4, CoO and Co phases during in situ PXRD reduction of the catalysts, Co/TiO_2 (a,d), $Co/TiO_2@mSiO_2$ (b,e) and $CoRu/TiO_2@mSiO_2$ (c,f).

was observed for the catalysts coated with the mesoporous silica structural promoter. It was however observed that when the reduction temperature was increased from 350 to 450 °C for the uncoated catalyst precursor (Co/TiO_2) the FT activity of this catalyst decreased at both reaction temperatures (220 °C –250 °C). This behaviour is attributed to possible sintering of the catalyst particles with increasing reduction temperature. In contrast, the increased FT activity for $Co/TiO_2@mSiO_2$ and $CoRu/TiO_2@mSiO_2$ with reduction temperature is due to the in-creased percentage reducibility at 450 °C and the stabilizing effect of the silica shell which hindered the propensity of the Co nanoparticles to sinter It is worth noting that the silica shell did not appear to hinder the mobility of the reactants and products to/from the Co catalyst Studies have shown that an increase in the catalyst reduction temperature can increase the catalytic activity but the problem of catalyst particle sin-tering then becomes dominant [33].

Comparison of the activity of the two catalysts $Co/TiO_2@mSiO_2$ and Co/TiO_2 at a reaction temperature of 220 °C and a the reduction tem-perature of 350 °C showed that at these temperatures that the silica shell played a role in lowering the Co activity. This is thought to be due to silica interacting with the Co nanoparticles. The effect of the SiO_2 was also observed at both higher reduction temperatures (450 °C) and higher reaction temperatures (250 °C). Here, however, the increased activities at the higher temperatures can be explained by reduced sin-tering due to the silica overlayer when compared to the Co/TiO_2 cat-alyst.

We can thus conclude that the reduction of the Co_3O_4 at 350 °C did not induce appreciable sintering of the Co particles on Co/TiO_2; and that the resulting difference in catalytic activity between Co/TiO_2 and $Co/TiO_2@mSiO_2$ after reduction at 350 °C at a reaction temperature of 220 °C is due to the coating of the catalyst with the oxidic silica shell and this limited the reduction of $Co/TiO_2@mSiO_2$. This showed that without adequate reduction, the silica shell can lower the catalytic activity while serving as a sinter resistant agent for the supported metal nanoparticles, $CoRu/TiO_2@mSiO_2$ gave high activity throughout [11]. The higher FT activity of $Co/TiO_2@mSiO_2$ relative to Co/TiO_2 at a reaction temperature of 250 °C and at both reduction temperatures can

Table 3
Fischer-Tropsch performance of the catalysts.

Catalyst	Reduction temperature (°C)	Reaction Temperature (°C)	CO Conversion (%)	Activity ($mol_{CO}\ g^{-1}_{Co}h^{-1}$)	Selectivity (C mol)%			STY, gC_{5+}/kg Me*h	$\propto^a$
					C_1	C_2-C_4	C_{5+}		
CoRu/TiO2@mSiO2	350	220	31.6	0.024	14.3	12.1	73.5	414	0.72
		250	53.0	0.053	29.6	23.3	47.1	446	0.57
	450	220	35.4	0.026	17.4	16.4	66.1	417	0.72
		250	58.9	0.065	25.8	21.9	52.2	550	0.67
Co/TiO2@mSiO2	350	220	17.0	0.010	7.9	5.2	86.8	249	0.71
		250	41.3	0.032	27.0	21.7	51.2	338	0.64
	450	220	22.2	0.012	10.1	9.3	80.6	303	0.74
		250	46.1	0.033	31.3	21.3	47.3	368	0.63
Co/TiO2	350	220	27.5	0.014	8.3	10.6	81.0	333	0.73
		250	36.6	0.021	23.9	15.9	60.1	330	0.61
	450	220	18.6	0.010	7.7	14.9	77.3	215	0.74
		250	33.1	0.018	24.5	20.9	54.5	269	0.59

α- Estimated by the ASF equation using liquid alkane products from C_9- C_{20}.

be further explained by sintering of the uncoated Co nanoparticles upon increasing the reaction temperature from 220 to 250 °C [6,36].

As expected the results indicate that the higher reduction tem-perature gives a catalyst with a lower dispersion of active metal na-noparticle, due to particle agglomeration. However the effect of the strong metal-support interaction (SMSI) can be overcome by the higher reduction temperature for the coated catalyst precursors. It is therefore seen that the reduction temperature of 450 °C was not high enough to produce a significant SMSI between the Co/TiO_2 and the silica shell [24]. The increased Fischer-Tropsch activity of the catalysts (Co/TiO_2@ $mSiO_2$ and $CoRu/TiO_2$@$mSiO_2$) after reduction at 450 °C showed that the catalysts did not undergo any deactivation by formation of SMSI. Nobile et al. have shown that for a Fe/TiO_2 (Degussa P-25 TiO_2) cata-lyst that an increased metal support interaction came into play at re-duction temperatures equal or above 450 °C [32]. However, for our catalysts, significant interactions that could lower the activity of the catalysts were not observed at 450 °C. This can be due to the fact that the SMSI interactions due to the titania support are not the same for supported Co or Fe nanoparticles. The in situ PXRD also showed no clear sign of the formation of $CoTiO_3$ up to 600 °C.

In addition, it should be noted that the catalyst reduction time had a significant bearing on the formation of the SMSI since it was observed that reduction of the catalysts at 450 °C for 6 h gave a catalyst that showed no FT activity. For Co/TiO_2 reduced at 450 °C, post synthesis analysis by XRD showed no Co peak or phase, attributed to the for-mation of mixed metal oxides at the higher reduction temperatures (Fig. S.9).

In summary, the reduction temperature, time and the ease with which the Co particles can agglomerate all contributed to the Co/TiO_2 showing lower FT activity after reduction at a higher temperature (450 °C). This phenomenon was not observed for the silica coated cat-alysts because of the protective shell. Nobile studied the effect of re-duction temperature on Fe/TiO_2 and observed that at temperatures $\geq$450 °C, there was an increase in SMSI by titania grain enlargement that lowered the catalyst active sites due to the formation of $FeTiO_x$ [32]. Work by Duvenhage et al. [37], showed that at reduction tem-peratures of 400 °C, the activity of a bimetallic $CoFe/TiO_2$ catalyst Fi-scher-Tropschwas lower than that of a catalyst reduced at a lower temperature of 300 and 350 °C. This was due to the deactivation me-chanism as suggested by Nobile and Davis [32], a mechanism that would not be evident on the silica coated catalysts.

TEM images of the catalyst after reaction ($CoRu/TiO_2$@$mSiO_2$), which had the highest activity of the coated catalysts did not show any silica shell breakage after Fischer-Tropsch synthesis (100 h at 220 and 250 °C; Fig. S.10).

3.4.2. Catalyst selectivities

Methane is the most stable Fischer-Tropsch product and tends to form in large quantities on Co catalysts [38]. Increased methane se-lectivity in FT studies always results in lower selectivity to high mole-cular weight products (i.e. C_{5+}). Cobalt Fischer-Tropsch catalysts per-form optimally (in terms of selectivity) at low temperatures and hence give the increased methane selectivity at 250 °C, relative to the data collected at 220 °C.

Fischer-Tropsch catalytic measurements showed that the silica coating did not have a significant effect on the catalyst hydrocarbon selectivity (Table 3). High reaction temperatures resulted in a high methane selectivity but the space time yield (STY) of the C_{5+} is still seen to be high when compared to the yield (STY) obtained at 220 °C for all the individual catalysts. From these studies we can infer that the effect of the SiO_2 on the Co particles does not result in significant dif-ferences in catalyst selectivity. The Ru promoted catalyst displayed a higher activity and higher methane content. This is because the Ru nanoparticles can increase the hydrogenation rates by hydrogen spil-lover (or its promoter effect on the Co nanoparticles) [30,39]. This process increased the termination step on the C_1 monomers thus lowering the chain growth probability. With increasing CO conversion methane selectivity decreased on $CoRu/TiO_2$@$mSiO_2$ while it was ob-served that the methane selectivity increased for Co/TiO_2@$mSiO_2$.

The difference in hydrocarbon selectivity for the catalysts reduced at temperatures of 350 and 450 °C can be accounted for by the in-creased activity of the catalysts. The selectivity for C_2-C_4 gaseous hy-drocarbons (between 5–25%) increased with FT reaction temperature and reduction temperature. The increased activity of the catalyst $CoRu/ TiO_2$@$mSiO_2$ was accompanied by higher yields of C_{5+} products (in terms of STY) when compared to the two catalysts which were not promoted with Ru. No specific trend in the hydrocarbon selectivities of the catalysts at Fischer-Tropsch synthesis of 250 °C was noted. At this reaction temperature and for a reduction temperature of 450 °C the catalyst Co/TiO_2@$mSiO_2$ gave higher methane selectivity than the $CoRu/TiO_2$@$mSiO_2$. However, at 220 °C the C_{5+} hydrocarbon (in terms of STY) decreased with increasing FT activity.

4. Conclusions

This study was aimed at designing stable Co catalysts for Fischer-Tropsch synthesis using a mesoporous silica shell as the structural promoter. A thin layer of silica was successfully coated onto the Co nanoparticles supported on TiO_2. The increased metal support inter-actions that can lower the reducibility of the catalysts were countered by using a Ru promoter. In situ XRD reduction studies and crystallite size calculations (of the Co phases) using the modified Scherrer equa-tion showed that the catalyst reduction followed the classical phase transformation from Co_3O_4 to Co via the CoO intermediate phase and that crystallite growth under the reduction conditions was only ob-served after complete transformation to Co phase. The Co metal growth was more pronounced on the uncoated Co/TiO_2 than for the silica coated catalysts. Fischer-Tropsch catalytic behavior of the catalysts was consistent with characterization data, and furthermore the use of a Ru promoter helped in giving a highly active sinter resistant catalyst.

This study showed that a triphasic compact nanoreactor can po-tentially be used in Fischer-Tropsch catalysis without effecting sig-nificant changes in the inherent Co nanoparticle activity and selectivity and that the Co nanoparticles propensity to sinter under high activity reaction conditions could be limited.

Acknowledgements

We wish to thank the NRF, the DST-NRF Centre of Excellence in Catalysis and the University of the Witwatersrand for financial support. The NNEP is also thanked for an equipment grant.

Appendix A. Supplementary data

Supplementary material related to this article can be found, in the online version, at doi:https://doi.org/10.1016/j.apcata.2017.12.015

References

[1] A.Y. Khodakov, W. Chu, P. Fongarland, Chem. Rev. 107 (2007) 1692–1744.
[2] H. Xiong, L.L. Jewell, N.J. Coville, ACS Catal. 5 (2015) 2640–2658.
[3] A. Jean-Marie, A. Griboval-Constant, A.Y. Khodakov, F. Diehl, Comptes Rendus Chimie 12 (2009) 660–667.
[4] M. Hauman, A. Saib, D. Moodley, E. Du Plessis, M. Claeys, E. Van Steen, ChemCatChem 4 (2012) 1411–1419.
[5] G. Jacobs, W. Ma, B.H. Davis, Catalysts 4 (2014) 49–76.
[6] M. Claeys, M. Dry, E. van Steen, P. van Berge, S. Booyens, R. Crous, P. van Helden, J. Labuschagne, D. Moodley, A. Saib, ACS Catal. 5 (2015) 841–852.
[7] N.E. Tsakoumis, M. Rønning, Ø. Borg, E. Rytter, A. Holmen, Catal. Today 154 (2010) 162–182.
[8] K. Fei Tan, J. Xu, J. Chang, A. Borgna, M. Saeys, J. Catal. 274 (2010) 121–129.
[9] A.M. Saib, D.J. Moodley, I.M. Ciobîcă, M.M. Hauman, B.H. Sigwebela, C.J. Weststrate, J.W. Niemantsverdriet, J. van de Loosdrecht, Catal. Today 154 (2010) 271–282.
[10] T.O. Eschemann, K.P. de Jong, ACS Catal. 5 (2015) 3181–3188.

[11] P. Lu, C.T. Campbell, Y. Xia, Nano Lett. 13 (2013) 4957–4962.
[12] Y. Wang, J. Liu, P. Wang, C.J. Werth, T.J. Strathmann, ACS Catal. 4 (2014) 3551–3559.
[13] J. Lu, B. Fu, M.C. Kung, G. Xiao, J.W. Elam, H.H. Kung, P.C. Stair, Science 335 (2012) 1205–1208.
[14] C. Chen, J. Qu, C. Cao, F. Niu, W. Song, J. Mater. Chem. 21 (2011) 5774–5779.
[15] N. Cheng, M.N. Banis, J. Liu, A. Riese, X. Li, R. Li, S. Ye, S. Knights, X. Sun, Adv. Mater. 27 (2015) 277–281.
[16] J.-G. Oh, H.-S. Oh, W.H. Lee, H. Kim, J. Mater. Chem. 22 (2012) 15215–15220.
[17] A.S. Reddy, S. Kim, H.Y. Jeong, S. Jin, K. Qadir, K. Jung, C.H. Jung, J.Y. Yun, J.Y. Cheon, J.-M. Yang, Chem. Commun. 47 (2011) 8412–8414.
[18] K. Yoon, Y. Yang, P. Lu, D. Wan, H.C. Peng, K. Stamm Masias, P.T. Fanson, C.T. Campbell, Y. Xia, Angew. Chem. Int. Ed. 51 (2012) 9543–9546.
[19] J.W. Geus, A.J. Dillen, Handbook of Heterogeneous Catalysis, (1997).
[20] Z. Bo, T.R. Eaton, J.R. Gallagher, C.P. Canlas, J.T. Miller, J.M. Notestein, Chem. Mater. 27 (2015) 1269–1277.
[21] C. Galeano, R. Güttel, M. Paul, P. Arnal, A.H. Lu, F. Schüth, Chem. Eur. J. 17 (2011) 8434–8439.
[22] G. Jacobs, T.K. Das, Y. Zhang, J. Li, G. Racoillet, B.H. Davis, Appl. Catal. A Gen. 233 (2002) 263–281.
[23] M. Voß, D. Borgmann, G. Wedler, J. Catal. 212 (2002) 10–21.
[24] J. Van de Loosdrecht, A. Van der Kraan, A. Van Dillen, J. Geus, Catal. Lett. 41 (1996) 27–34.
[25] G.R.M. Melaet, W.T. Ralston, C.-S. Li, S. Alayoglu, K. An, N. Musselwhite, B. Kalkan, G.A. Somorjai, J. Am. Chem. Soc. 136 (2014) 2260–2263.
[26] R. Xie, C. Wang, L. Xia, H. Wang, T. Zhao, Y. Sun, Catal. Lett. 144 (2014) 516–523.
[27] F. Morales, B.M. Weckhuysen, Catalysis 19 (2006).
[28] S.K. Beaumont, S. Alayoglu, C. Specht, W.D. Michalak, V.V. Pushkarev, J. Guo, N. Kruse, G.A. Somorjai, J. Am. Chem. Soc. 136 (2014) 9898–9901.
[29] W.C. Conner Jr., J.L. Falconer, Chem. Rev. 95 (1995) 759–788.
[30] J. Hong, E. Marceau, A.Y. Khodakov, L. Gaberová, A. Griboval-Constant, J.-S. Girardon, C.L. Fontaine, V. Briois, ACS Catal. 5 (2015) 1273–1282.
[31] R. Cheary, J. Res. Natl. Inst. Stand. Technol. 109 (2004).
[32] A. Nobile, M. Davis, J. Catal. 116 (1989) 383–398.
[33] M.K. Rayner, D.G. Billing, N.J. Coville, Acta Crystallogr. Sec. B Struct. Sci. Cryst. Eng. Mater. 70 (2014) 498–509.
[34] H.E. du Plessis, R.P. Forbes, W. Barnard, W.J. Erasmus, A. Steuwer, Phys. Chem. Chem. Phys. 15 (2013) 11640–11645.
[35] T.N. Phaahlamohlaka, D.O. Kumi, M.W. Dlamini, R. Forbes, L.L. Jewell, D.G. Billing, N.J. Coville, ACS Catal. 7 (2017) 1568–1578.
[36] B.H. Davis, M.L. Occelli, Advances in Fischer-Tropsch Synthesis, Catalysts, and Catalysis, CRC Press, 2009.
[37] D. Duvenhage, N. Coville, Appl. Catal. A Gen. 233 (2002) 63–75.
[38] G.P. Van Der Laan, A. Beenackers, Catal. Rev. 41 (1999) 255–318.
[39] D. Nabaho, J.H. Niemantsverdriet, M. Claeys, E. van Steen, Catal. Today 261 (2016) 17–27.